Vol. 05, No. 2 (2023) 311-324, doi: 10.24874/PES05.02.014

Proceedings on Engineering Sciences

www.pesjournal.net

CLASSIFYING OF MRI IMAGES FOR CEREBRAL TUMOR USING SOFT COMPUTING TECHNIQUES

Bhavna Pancholi[1]
Pramod Modi
Nehal Chitaliya

Received 13.11.2022.
Accepted 17.02.2023.
UDC – 004.932.4

Keywords:

MRI images, Brain Tumor, Pre-processing, Image Segmentation, Feature Extraction

A B S T R A C T

Healthcare scientists determined how MRI images have indeed been highly beneficial in latest times in the investigation of the recognition and early identification of a brain disease. The main primary stages in analyzing the brain MRI pictures are image pre-processing, segmentation, feature extraction, and classification. Among the crucial processes that can evaluate how well brain MRI scans can be classified and ultimately the condition it will indicate is feature extraction and segmentation. In this paper stage wise methods are described. In the first stage (pre-processing stage) different filters; like; median, weiner, anistropic, non local means as well as combined filters used. In the pre-processing part, combined weiner and anistropic filter gives the best result. In the second stage (segmentation stage), multi-thresholding technique – cuckoo search algorithm used using different objective functions; like; ostu, kapur entropy, tsallis entropy and proposed. In the proposed method of the segmentation stage used cuckoo search algorithm using combined ostu and tsallis entopy as an objective function. In the third stage (feature extraction), discrete wavelet transform used and in the fourth stage (classification) support vector machine used. In each stage results are compared using different parameters and we got best output using proposed method.

1. INTRODUCTION

One of the difficult problems in image processing is noise elimination, which deals with the restoration and image improvement of a digital image which has become distorted by noise during gathering, preservation, or dissemination. It is an unavoidable effort to eliminate or at least reduce noise in pictures. Perhaps a small amount

The primary widely used diagnostic tools are medical images generated from ultrasound (US) imaging, MRI and CT scan and due to its non-invasive, safe, and precise nature. Furthermore, photo collection and equipment may bring up unwanted interruptions like speckle distortion, salt and pepper, Poisson and Gaussian noises. Due to the drastic degradation of optical measurements, like image density and intensity, it is difficult to distinguish among regular and diseased cells in medical studies. Therefore, a necessary preprocessing step to achieve the best evaluation is to denoise medical data without changing limits, modifying essential parts of the images, or harming anatomical traits. Brain tumors and other cerebral

[1] Corresponding author: Bhavna Pancholi
Email: bhavana.p.pancholi-eed@msubaroda.ac.in

abnormalities can be diagnosed, graded, treated, and the effectiveness of the therapies can be evaluated using magnetic resonance imaging (MRI) (Chahal et al, 2020).

The categorization of brain tumors is a difficult issue in the realm of clinical picture analysis. The current research suggests a hybrid approach that makes use of neuro-physics and convolutional neural networks (NS-CNN) (Jia et al., 2020; Suresh et al., 2016). It seeks to distinguish between harmless and harmful tumor regions in sections separated from brain pictures. Initially, the neutrosophic group - master greatest fuzzy-sure entropy (NS-EMFSE) method was used to divide the MRI pictures. During the classification phase, CNN collected the characteristics of the fragmented brain pictures and evaluated them utilizing SVM and KNN algorithms. On 80 benign tumors and 80 malign tumors, an operational assessment predicated on 5-fold cross-validation is conducted. The results showed that CNN characteristics have excellent classification performance across a range of classifications (Rahaman et al., 2021; Yang et al., 2009).

While modelling findings verified source information with a mean accuracy rate of 95.62 percent, actual findings show that CNN characteristics demonstrated a superior categorization efficiency with SVM. By identifying brain tumors as harmless and malignant, the primary objective of this article is to develop an effective automated brain tumor separation method. NS-EMFSE was used to separate brain tumors. Alexnet collected the characteristics of the divided pictures using CNN structures, and SVM and KNN classifiers being used to determine their classification. The deep learning technique that uses feed-forward layers is CNN. The application utilized Matlab 2017b and the MatConvnet library. SVM classifier produced the best results, scoring 95.62% (Deng et al., 2022; Kalpana et al., 2020).

If more photos are utilized in the collection, it is predicted that this reliability percentage would rise. Research on segmentation and classification is among the least often discussed subjects in picture analysis. The renowned and effective segmentation and classification techniques CNN and Neutrosophy can be used, and this could significantly advance picture recognition. Intend to look into how distinct Neutrosophic methods using various CNN topologies affect classification reliability in upcoming research. Depending on a convolutional neural network with neutrosophic professional maximum fuzzy sure entropy, a brain tumor identification algorithm.

Figure 1 indicates stage wise block diagram of the proposed system. Theoretical aspects given in the section – 2. Results given in the section – 3. Conclusion given in the Section – 4.

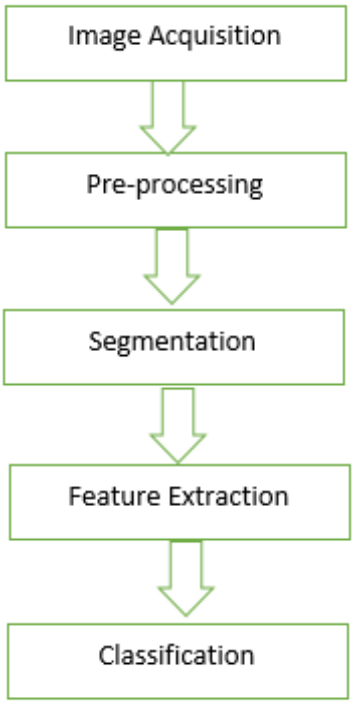

Figure 1. Block diagram of the proposed system

2. THEORETICAL ASPECT OF TECHNIQUES

In the pre-processing part, there are several filters used for noise removal, like; Median, Wiener, Anisotropic Diffusion filter, Non Local Means etc (Mahmud Boby et al., 2021; Perona, P et al., 1990). In this the Wiener filter is widely implemented to minimize the amount of distortion in a scan by relating it to an estimate of required noise free signal. It employs a statistical technique. Because of its simplicity and quickness, the Wiener filter is widely used and gives good output compare to other filters. Also combination of the different filters used for more accurate results. In this paper different combination of the combined filters are used for pre-processing of an image; like; combined weiner and anistropic, combined weiner and median, combined weiner and non local means. In this combined weiner and anistropic gives best output.

There are so many techniques are used for image segmentation. In this thresholding is the one of the technique used for image segmentation. There are two types of thresholding; one is bi-level thresholding and other is multi-level thresholding (Rahaman et al., 2021). Compare to the bi-level thresholding techniques, multi-level thresholding techniques gives good performance. There are so many different algorithm are used in the multi-level thresholding techniques. One of the algorithm is cuckoo search algorithm. In the cuckoo search algorithm, different objective functions are used for optimum output (Suresh et al., 2016).

2.1. Cuckoo search (CS) algorithm:

The cuckoo search algorithm was proposed by (Yang et al, 2009) and is a metaheuristic method. The CS imitates the cuckoo's egg-laying operation. Cuckoos typically lay their fertilised eggs in host nests in the hopes that they would be nurtured by substitute parents in spring. The host may recognise that the eggs in their nests are not their own occasionally. In these situations, either the entire nest is thrown out or the foreign eggs are removed from the nests. The CS optimization algorithm is generally based on the following three principles:

1. It's interesting to note that each cuckoo bird only lays one egg at a time, which it randomly inserts in the nest of a host bird.
2. Typically, the best nests with top-notch eggs are passed down to the following generations.
3. There are a fixed number of host nests available. With probability p_a, the host bird finds foreign eggs with a probability that ranges from 0 to 1. Keep in mind that the best nests are chosen for the subsequent calculations. For the sake of simplicity, principle 3 can be described as follows: with probability p_a, new nests will replace the existing n nests.

The CS method can be distilled into the following three ideas based on these three principles:

A Lévy light is carried out while producing new solution x_i^{t+1} for cuckoo I (8):

$$x_i^{t+1} = x_i^t + \alpha_0 (x_i^t - x_{best}) \oplus Levy(\lambda) \quad (1)$$

Where x_{best} denotes the current best solution, $\oplus$ Element-wise multiplication, and α_0 is the step size $\alpha_0 > 0$.

Levy flights are selected using a Levy distribution, which is given by:

$$Levy(\lambda) \sim u = t^{-\lambda}, (1 < \lambda \leq 3) \quad (2)$$

Based on the breeding behaviour of several cuckoo species, we have developed a new metaheuristic called Cuckoo Search in conjunction with L'evy flights in this work. Show that CS is better than other metaheuristic algorithms based on the literature review. Studying multiobjective optimization applications is a simple extension of the possibly effective optimization method. Levy step size and x_{best} are the main challenges of the cuckoo search algorithm. x_{best} is found using optimization. Different methods are used to maximize the function, like; using Ostu's method, using Kapur entropy method, using Tsallis entropy method, etc.

2.2. Proposed cuckoo search (CS) algorithm:

Otsu's presumption of binary classes is its major drawback: The grayscale histogram is divided into two classes. However, in real-world segmentation problems we most generally deal with images having more than two class of segments. According to the literature review, employing the Otsu approach for CS results in lower PSNR values than utilising Kapur's entropy. Because Tsallis entropy is non-extensive, when two identical systems unite, the combined system's entropy is not equal to the sum of the entropies of its subsystems. Compare to CS using Kapur's entropy method Tsallis entropy gives higher PSNR values and other parameters. The long-range correlations in an image can be described using the non-extensive entropy technique. The range of its use is constrained by the fact that, like other entropy-based algorithms, it is still extremely sensitive to the disturbance of signals. For small target extraction, the Otsu method is more reliable but less precise. The benefits of the two can thus be combined to create a new algorithm with a broader range of applications. We proposed new method, combined Otsu and Tsallis entropy as an objective function to find the x_{best}.

The long-range correlations in an image can be described using the non-extensive entropy technique. The range of its use is constrained by the fact that, like other entropy-based algorithms, it is still extremely sensitive to the disturbance of signals. For small target extraction, the Otsu method is more reliable but less precise. The benefits of the two can thus be combined to create a new algorithm with a broader range of applications. Noting that information redundancy now governs the non-extensive parameter q in Tsallis entropy and cannot be set arbitrarily.

A new objective function is denoted by:

$$\mu(t) = S_q^{a+b} + (\sigma_W^2)^{1-q} \quad (3)$$

$q > 0$ needs to be met in order to maintain the concavity of Tsallis entropy (Tsallis et al., 1988). In contrast, $q < 1$ is referred to as superextensivity, which raises the system's overall entropy in compared to the extensive case ($q = 1$) (Tsallis et al., 1998). Practically speaking, practically all kinds of images display the superextensivity feature (Ramírez-Reyes et al, 2016). Consequently, $0 < q < 1$ can be the appropriate range for the non-extensive parameter. We can see that each of the two strategies are designed to maximise the objective functions.. Equations 3's goal is to increase the objective function.

$$t^* = Arg\ max\{\mu(t)\} \quad (4)$$

With the range of q stated above, equation 4 yields the ideal threshold. The profile of each peak is the normalised q-Gaussian distribution function for a synthetic image with a bimodal histogram distribution, as shown in Figure 2 (Huang et al., 2013). We can see that the best threshold for the Otsu algorithm and the Tsallis entropy algorithm is the valley gray-level between the two peaks, which exactly matches the outcome of equation 4. There is no proof that the result of ostu and tsallis entropy

coincide for other natural photographs with an arbitrary histogram distribution, however equation 3 shows a trade-off between them and equation 4 may produce an appropriate proposal. It should be noted that S_q^{a+b} and σ_W^2 have extremely different magnitudes in the histogram of Figure 2. Both of them are functions of threshold t, as illustrated in Figure 3. The Otsu method, however, completely suppresses the Tsallis entropy algorithm's outputs for any conceivable threshold t. Consequently, it is inappropriate to directly combine S_q^{a+b} and σ_W^2.

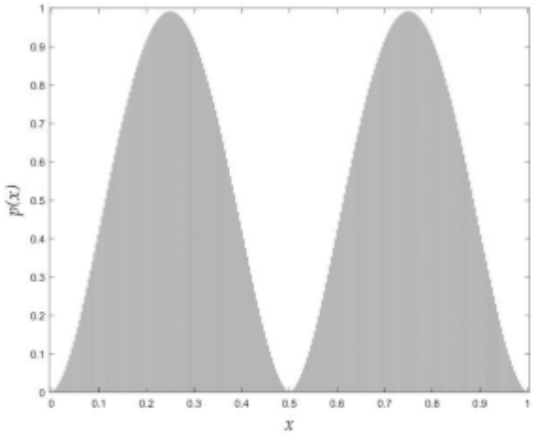

Figure 2. Normalized histogram distribution

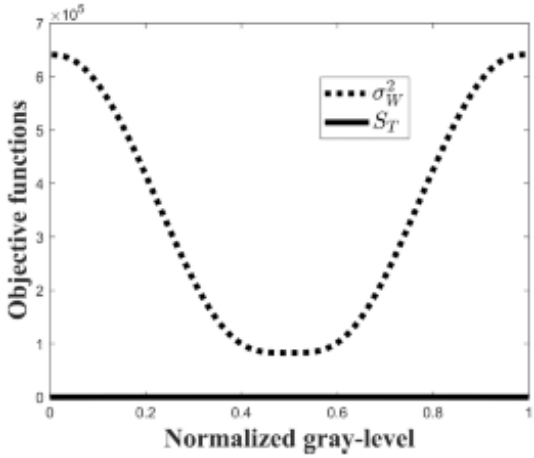

Figure 3. Objective functions of the Ostu and Tsallis algorithms

The magnitude of σ_W^2 can be revised using the q-exponential function (Ou Congjie et al., 2010) to minimise the effects of the magnitude difference. With a continuous probability distribution function, Tsallis entropy is defined as:

$$S_T = \frac{1-\int_0^1 p(x)^q\,dx}{q-1} \tag{5}$$

where the probability density of the normalised gray-level value is denoted by p(x). The appropriate probability distribution for a system with non-extensive q-entropy can be expressed as the q-Gaussian function (Huang et al, 2013),

$$p(x) = \frac{1}{Z_q}\left[1-(1-q)\frac{x^2}{\sigma^2}\right]^{\frac{1}{1-q}} \tag{6}$$

If Zq is the partition function to maintain the probability normalisation requirement and σ^2 is the variance of x,

$$Z_q = \int_0^1 \left[1-(1-q)\frac{x^2}{\sigma^2}\right]^{\frac{1}{1-q}} dx = \frac{\sigma\sqrt{\pi}}{2\sqrt{1-q}}\frac{\Gamma\left(1+\frac{1}{1-q}\right)}{\Gamma\left(\frac{3}{2}+\frac{1}{1-q}\right)} \tag{7}$$

where factorial (k - 1)! will be reached from the Gamma function Γ(k) assuming k is a number. Adding p(x) to equation 18 results in:

$$S_T = \frac{1-\int_0^1 \frac{1}{Z_q^q}\left[1-(1-q)\frac{x^2}{\sigma^2}\right]^{\frac{q}{1-q}} dx}{q-1} = \frac{1-\xi(\sigma^2)^{\frac{1-q}{2}}}{q-1} \tag{8}$$

where:

$$\xi = \left[\frac{\pi}{4(1-q)}\right]^{\frac{1-q}{2}}\left[\frac{\Gamma\left(\frac{3}{2}+\frac{1}{1-q}\right)}{\Gamma\left(1+\frac{1}{1-q}\right)}\right]^q \frac{\Gamma\left(\frac{1}{1-q}\right)}{\Gamma\left(\frac{3-q}{2(1-q)}\right)} \tag{9}$$

is the integration constant for a given value of q. According to the non-extensivity of Tsallis entropy, if If p_a and p_b are two identical q-Gaussian distribution functions, the total entropy can be expressed as follows:

$$S_T(a+b) = S_T(a) + S_T(b) + (1-q)S_T(a)S_T(b)$$

$$S_T(a+b) = \frac{1-\xi_a(\sigma_a^2)^{\frac{1-q}{2}}}{q-1} + \frac{1-\xi_b(\sigma_b^2)^{\frac{1-q}{2}}}{q-1} + (1-q)\frac{1-\xi_a(\sigma_a^2)^{\frac{1-q}{2}}}{q-1}\frac{1-\xi_b(\sigma_b^2)^{\frac{1-q}{2}}}{q-1} \tag{10}$$

Substituting $\sigma_a^2 = \sigma_b^2 = \sigma_W^2$ into equation 23 yields:

$$S_T(a+b) = \frac{\xi_a\xi_b(\sigma_W^2)^{1-q}-1}{1-q} \tag{11}$$

Therefore, the magnitude of $(\sigma_W^2)^{1-q}$ is comparable with $S_T(a+b)$ at the proper range of q, and the rationality of equation 3 is shown.

In the feature extraction part, different methods used, like; Stationary Wavelet Transform (SWT), Discrete Wavelet Packet Transform, and Discrete Wavelet Transform (DWT)(Raut et al., 2014). The objective of the textured elements separation employing the DWT is to classify the picture by gathering additional factors from the matrix picture which contain specific data. A technique has successfully employed to represent the Gaussian dispersion of wavelet components. The characteristics that are deconstructed by DWT, such as approximated, horizontal information, lateral specifics, and diagonal description, were subjected to a straightforward statistical technique in the suggested technique employing the Standard Deviation parameter.

In the classification part, there are different methods used for image classification, like; SVM, GLCM, CNN etc. In this paper SVM method used for image classification. (Çinar et al., 2020, Rao et al., 2022).

3. RESULT ANALYSIS

3.1 pre-processing

The description of parameters implemented for 7 images is given below:

3.1.1. Peak signal to noise ratio (PSNR)

The PSNR is the proportion of utmost attainable signal intensity to distorted noise signal intensity. The statistic used to evaluate it is the decibel (dB). For reconstructed distorted photos, it is the most often utilized quality assessment measure (V. Anoop, 2019). The noise is a byproduct of reducing or deforming the signal, which is the actual data. PSNR is shown as:

$$PSNR= 10 \log 255^2/MSE \tag{12}$$

3.1.2. Mean square error (MSE)

Among the two monochrome images P and Q, one is real and the other is contrived. The input image, pij, and the filtered output image, qij, are both M x N in dimension. Summarizing the values of I and j represents the total number of pixels in the images, whereas M and N represent the number of rows and columns in the primary images (V. Anoop, 2019). MSE is used to determine the mean of the squares of the variance in a source and screened scan. The dimension is at its smallest when the photographs are nearly similar. The more MSE there are, the better it is for figuring out how much the image has improved.

$$\text{MSE} = \frac{\sum_{j=1}^{N}\left(\sum_{i=1}^{M}(p_{ij}-q_{ij})^2\right)}{MN} \tag{13}$$

3.1.3. Root mean square error (RMSE)

RMSE is a widely used inaccuracy measuring tool. It is a method that figures out the difference among the actual and predicted results (V. Anoop, 2019). The final result of RMSE often indicates the intensity of the variation and is unfavorable. RMSE is square root of MSE. Higher performance is attained if RMSE is less than a certain value.

$$RMSE = \sqrt{MSE} \tag{14}$$

3.1.4. Universal quality index (UQI)

A statistic is described as "global" since it is unaffected by the conditions under which it was observed. The ideal outcome although is 1 and the dynamic scale is (-1,1). It corrects for incoherence, brightness distortion, and intensity disturbance in one parameter (V. Anoop, 2019). Assume that $p = \{p_i \mid i = 1, 2, \dots \dots N\}$ and $q = \{q_i \mid i = 1, 2, \dots \dots N\}$ is the real and assessed image values, respectively. According to the suggested quality index's description:

$$UQI = \frac{4\,\sigma_{pq}\,\bar{p}\,\bar{q}}{(\sigma_p^2+\sigma_q^2)(\bar{p}_+^2\,\bar{q}^2)} \tag{15}$$

here,

$$\bar{p} = \frac{1}{N}\sum_{i=1}^{N} p_i \;, \bar{q} = \frac{1}{N}\sum_{i=1}^{N} q_i$$

$$\sigma_p^2 = \frac{1}{N-1}\sum_{i=1}^{N}(p_i-\bar{p})^2 \;, \quad \sigma_q^2 = \frac{1}{N-1}\sum_{i=1}^{N}(q_i-\bar{q})^2$$

$$\sigma_{pq} = \frac{1}{N-1}\sum_{i=1}^{N}(p_i-\bar{p})\,(q_i-\bar{q})$$

In the research work implementation of the specific filters as well as the combining of filters is employed. The PSNR that is measured in dB and represents the best possible signal-to-deformed-noise ratio, ought to be higher in value. Different filters including Median, Weiner, Anisotropic, Non-Local Median (NLM) and the filter combinations are used to determine PSNR. The Weiner filter obtained the best results of all the individual filters. As a result, it was carried forward for more filter combinations.

Figure 4 reflects the mean result for five distinct cases of each filter. The PSNR of the Median Filter was 33.76693 dB, the Weiner filter is 41.83702 dB, the Anisotropic filter was 36.6281 dB and the NLM filter was 33.76159 dB. The PSNR of combined Weiner and NLM was 42.71564 dB, Weiner and Anisotropic was 50.33409 dB and Weiner and Median was 50.31828 dB while taking into account the combination of filters.

MSE is used to determine the mean square of errors for both the actual and intended scans. The MSE value, must be as low as possible to obtain an accurate image. In Figure 5, the MSE for each separate filter is determined, and the mean values for five distinct cases is shown. The Median filter had a Mean value of 28.82616, Weiner filter of 4.29316 dB, Anisotropic filter of 14.26918 and NLM filter of 27.56265. The MSE of the combined Weiner and NLM was 3.50684, Weiner and Anisotropic was 0.60684, and Weiner and Median was 0.60905 when the combination of filters was taken into account.

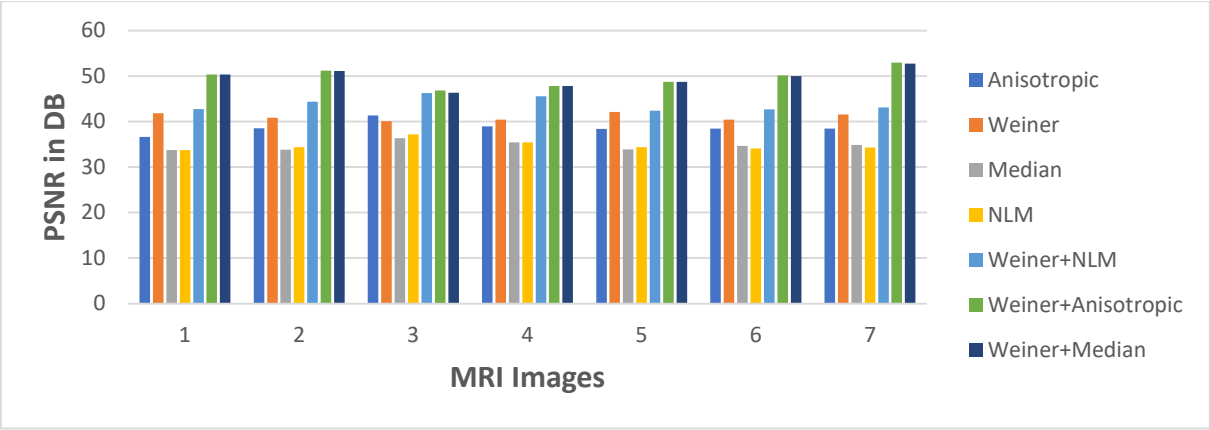

Figure 4. DICOM Image of the PSNR in dB for Median filter, Weiner filter, Anisotropic filter, NLM, Weiner and NLM, Weiner and Anisotropic and Weiner and Median

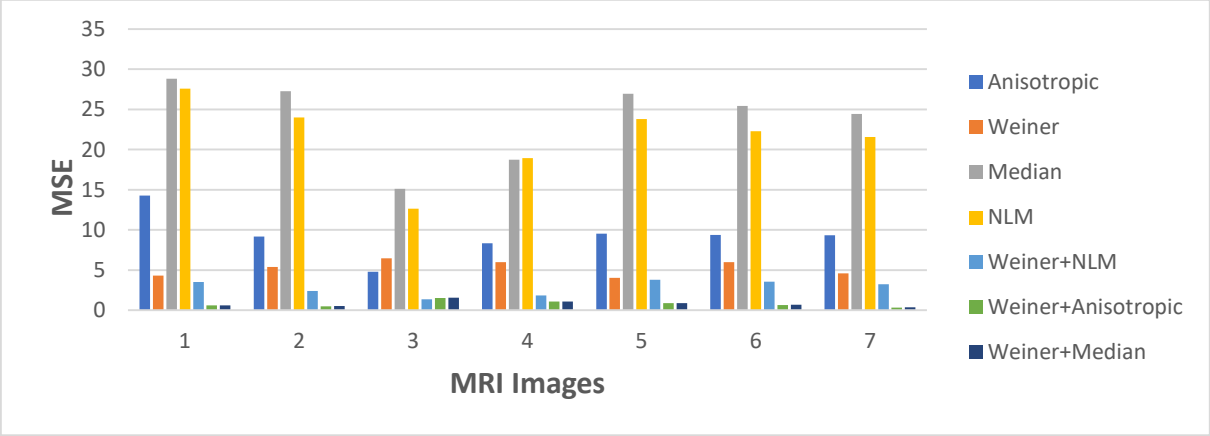

Figure 5. DICOM Image of the MSE in dB for Median filter, Weiner filter, Anisotropic filter, NLM, Weiner and NLM, Weiner and Anisotropic and Weiner and Median

It is common procedure to quantify inconsistency using the Root Mean Squared Error (RMSE), and must be kept to a low to ensure good output. Figure 6 shows the RMSE for each unique filter and the mean result for five distinct cases. The RMSE of the Median filter, Weiner filter, Anisotropic filter and NLM filter was 5.369, 2.0719, 3.77746 and 5.25001, respectively. Combined Weiner and NLM had RMSE value 1.87265, Weiner and Anisotropic had RMSE value 0.779, and Weiner and Median had RMSE value 0.78041 when the combination of filters is taken into account.

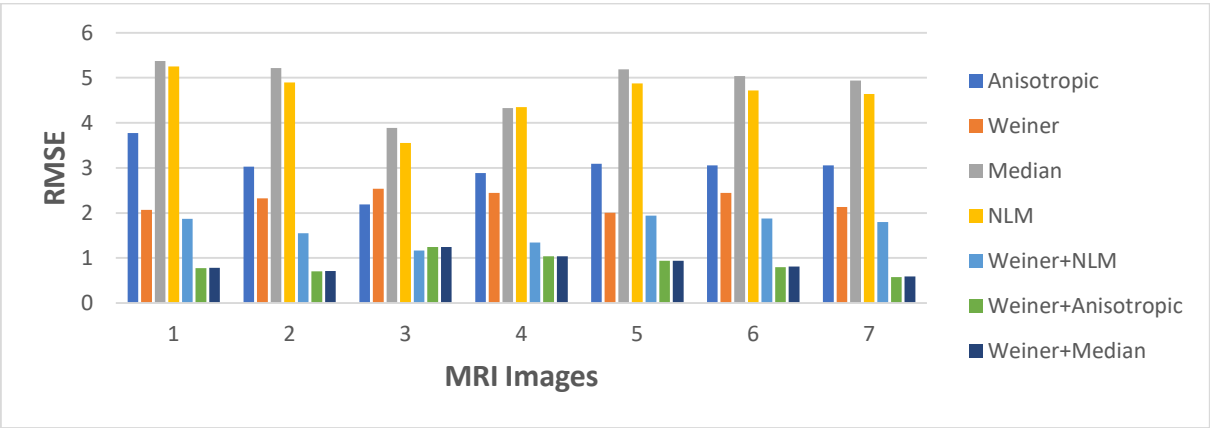

Figure 6. DICOM Image of the RMSE in dB for Median filter, Weiner filter, Anisotropic filter, NLM, Weiner and NLM, Weiner and Anisotropic and Weiner and Median

The Universal Image Quality Index (UQI) of the filter is evaluated in dB and is ought to be higher for improved noise - reducing quality. The single filter and mean values for five separate cases is shown in Figure 7. The UQI values of the Median Filter, Weiner Filter, Anisotropic Filter and NLM Filter was 0.55756, 0.76749, 0.77565 and 0.52635 respectively. The UQI result of combined Weiner and NLM was 0.75576, Weiner and Anisotropic was 0.81949, and Weiner and Median was 0.77949 when the combination of filters was taken into account.

In terms of statistical parametrs; PSNR, MSE, RMSE and UQI; combined Weiner and Anistropic filter gives best output.

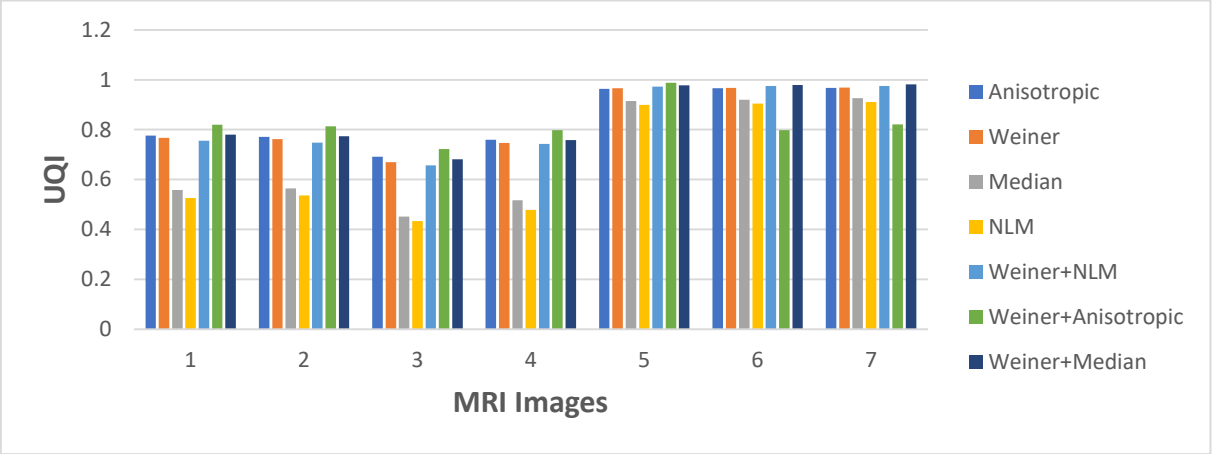

Figure 7. DICOM Image of the UQI in dB for Median filter, Weiner filter, Anisotropic filter, NLM, Weiner and NLM, Weiner and Anisotropic and Weiner and Median

3.2 Segmentation

Pre-processing and Segmentation image samples are shown in Figures 8 and 9. The Weiner Filter, Anistropic Filter and Weiner Filter & Anistropic Filter Pictorial Presentation is displayed in the front row of Figures 8 and 9. These filters are described theoretically in the section 3 along with their parameters like PSNR, MSE, RMSE & UQI with their equations. The segmentation output, which includes the Cuckoo Ostu Threshold, Cuckoo Kapur Threshold, Cuckoo Tsallis Threshold and Cuckoo Otsu & Tsallis Threshold is vividly represented. The proposed research demonstrates that when compared to various individual and combined filters, the Cuckoo Otsu & Tsallis entropy combination produces outstanding outcomes.

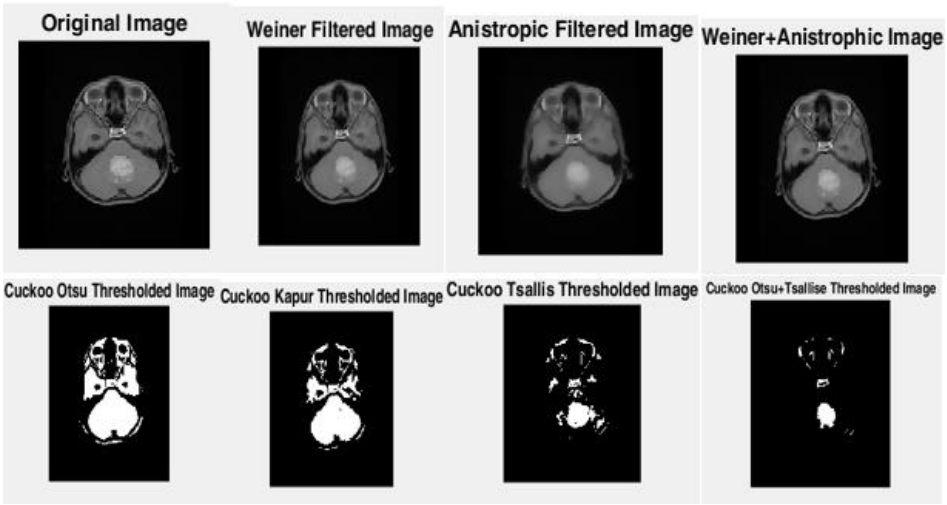

Figure 8. Pictorial Presentation of Pre-processing and Segmentation output of Weiner Filter, Anistropic Filter, Weiner Filter & Anistropic Filter, Cuckoo Ostu Threshold, Cuckoo Kapur Threshold, Cuckoo Tsallis Threshold and Proposed Method

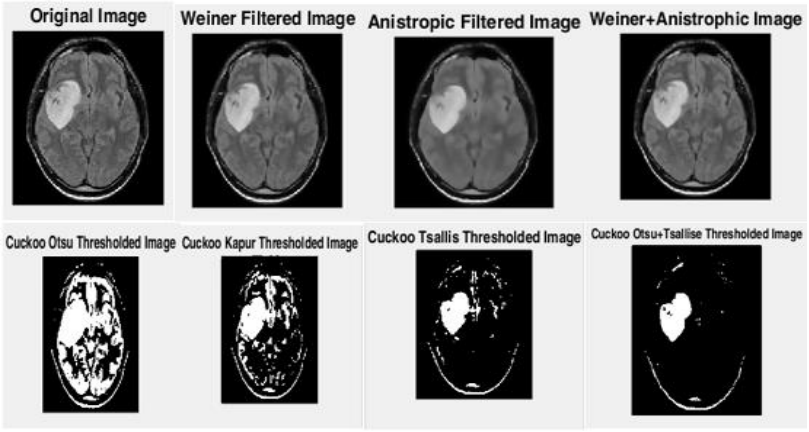

Figure 9. Pre-processing and Segmentation Output Images of Weiner Filter, Anistropic Filter, Weiner Filter & Anistropic Filter, Cuckoo Ostu Threshold, Cuckoo Kapur Threshold, Cuckoo Tsallis Threshold and Proposed method

3.3 Feature extraction

The description of parameters implemented for 7 images is given below (Vachan Vadmal et al, 2020):

3.3.1 mean

The intensity of a grey magnitude picture is typically measured statistically using the term mean (Raut et al, 2016).

$$\text{Mean} = \frac{1}{m+n}\sum_{x=0}^{m-1}\sum_{y=0}^{n-1} f(x,y) \quad (16)$$

3.3.2 Standard deviation

This variable displays the degree of "diffusion" from the median or anticipated intensity of the pixel. The significant standardized variation signifies that the data units are dispersed relatively randomly, whereas a low standardized variation indicates that the data units have a tendency to be near the mean (Raut et al, 2016).

The Standard Deviation is given by:

$$\text{Standard Deviation (SD)} = \sqrt{\frac{1}{m+n}\sum_{x=0}^{m-1}\sum_{y=0}^{n-1} (f(x,y)-\text{Mean})^2} \quad (17)$$

3.3.3 Variance

It evaluates neighbouring distinction and sums up the histogram dispersion (Raut et al, 2016). The divergence and dispersion from the average are greater the more the variance.

$$\text{Variance} = \sigma^2 = \sum_{x=0}^{m-1}\sum_{y=0}^{n-1} (x-\mu)^2 . (y-\mu)^2 . f(x,y) \quad (18)$$

3.3.4 Root mean square error

It calculates the discrepancy among the observed value that a system or classifier anticipated and the real value.

$$MSE = \frac{\sum_{j=1}^{N}\left(\sum_{i=1}^{M}(f_{ij}-y_{ij})^2\right)}{MN} \quad (19)$$

$$\text{RMSE} = \sqrt{\text{MSE}} \quad (20)$$

3.3.5 Entropy

This relates to the amount of energy which is constantly dissipated to heat whenever a process or structural transition takes place; the idea derives from thermodynamics. When grey values are dispersed evenly, perhaps with identical possibilities, a picture's entropy is at its highest (Jude Hemanth et al, 2012). Photos with minimal entropy have little content and poor picture resolution, whereas pictures with greater levels have more data and better features. Entropy can never be restored to be put to productive usage. As a result, the word might be interpreted as the degree of irreparable disarray or instability. The entropy of a grayscale picture can be described as:

$$\text{Entropy} = \sum_{x=0}^{m-1}\sum_{y=0}^{n-1} f(x,y)\log_2 f(x,y) \quad (21)$$

3.3.6 Skewness

It serves as a measure for symmetrical or, rather specifically, for asymmetry (Raut et al, 2016). When a distributed or set of data appears identical to the left and right of the centre, it is said to be symmetrical.

$$S_K = \frac{1}{m*n}\sum\frac{(f(x,y)-M)^3}{SD^3} \quad (22)$$

3.3.7 Kurtosis

It evaluates how heavy or light-tailed the information are in comparison to a statistical allocation.

$$K = \frac{1}{m*n}\sum\frac{(f(x,y)-M)^4}{SD^4} \quad (23)$$

3.3.8 Energy

It is consistency or angular second moment (ASM). The value increases with the homogeneity of the picture. The assumption is that the picture is a steady picture if energies is equivalent to 1 (Raut et al, 2016).

$$\text{Energy} = \sqrt{\sum_{x=0}^{m-1}\sum_{y=0}^{n-1} f^2(x,y)} \quad (24)$$

3.3.9 Contrast

Brightness or grey-level differences among the standard pixel and its neighbour are measured as contrast. Contrast in the actual globe is created by the contrast between one element as well as other things in the identical range of sight in colour and intensity. The unit is located on the diagonal therefore x- y = 0 if x and y are identical. Assuming a value of 0, such data indicate pixels that are identical to its neighbour in every way. There is a slight difference and the value is 1 if x and y vary by 1. The contrast is rising and the magnitude is four if x and y are varied by two. As (x,y) rises, the weights tend to rise rapidly (Raut et al, 2016).

$$\text{Contrast} = \sum_{x=0}^{m-1}\sum_{y=0}^{n-1}(x-y)^2\, f(x,y) \quad (25)$$

3.3.10 Correlation

The co-occurrence matrix grey level elements linear dependence is demonstrated by the correlation characteristic. It shows how closely linked a baseline pixel is to its neighbour's. Here 0 indicates no connection and 1 indicates an ideal one.

$$\text{Correlation} = \frac{\sum_{x=0}^{m-1}\sum_{y=0}^{n-1}((x,y)\, f(x,y)) - M_X M_Y}{\sigma_X \sigma_Y} \quad (26)$$

3.3.11 Inverse different moment (IDM)

IDM is typically referred to as homogeneity which evaluates the regional homogeneity of a picture. The assessments of the dispersion of GLCM component's proximity to the GLCM diagonal are obtained by the IDM characteristic. Its value obtained is the opposite of a Contrast weight having values falling off the diagonal progressively (Jude Hemanth et al, 2012).

$$\text{Inverse Difference Moment (IDM)} = \sum_{x=0}^{m-1}\sum_{y=0}^{n-1}\frac{1}{1+(x-y)^2}.f(x,y) \quad (27)$$

3.3.12 Homogeneity

It analyses the resemblance of pixels. The homogeneity of a diagonally grey layer co-occurrence vector is 1 (Raut et al, 2016). If just little modifications are made to localized texturing, it expands in size.

$$\text{Homogeneity} = \sum_{x=0}^{m-1}\sum_{y=0}^{n-1}\frac{f(x,y)}{1+|x-y|} \quad (28)$$

Table 1 presents the Overview of the parameters for 7 DICOM images in table format. The parameters covered are Contrast, Correlation, Energy, Homogeneity, Mean, Standard Deviation. Table 2 also presents the Overview of the other parameters for 7 DICOM images in table format. The parameters covered are Entropy, RMS, Variance, Smoothness, Kurtosis, Skewness & Inverse Different Moment (IDM).

Table 1. Overview of the parameters for 7 scans in table format

Image	Contrast	Correlation	Energy	Homogeneity	Mean	Standard Deviation
1	0.4088	0.1434	0.8548	0.9563	0.004	0.0897
2	0.3715	0.139	0.8433	0.9533	0.0035	0.0897
3	0.389	0.1593	0.8317	0.9506	0.0053	0.0897
4	0.4066	0.1487	0.8477	0.956	0.0057	0.0896
5	0.3793	0.1669	0.8421	0.9537	0.0054	0.0897
6	0.4577	0.1068	0.8457	0.9531	0.0062	0.0896
7	0.4049	0.1116	0.8298	0.9516	0.0064	0.0896

Table 2. Overview of the parameters for 7 scans in table format

Image	Entropy	RMS	Variance	Kurtosis	Skewness	Inverse Different Moment (IDM)
1	1.8996	0.0898	0.0081	34.5253	3.087	2.1595
2	1.9461	0.0898	0.0081	31.4948	2.6799	2.6068
3	2.0521	0.0898	0.0081	28.4069	2.7713	2.6796
4	2.0184	0.0898	0.008	36.449	3.3445	3.7778
5	1.9903	0.0898	0.0081	30.1213	2.9186	3.4326
6	1.9695	0.0898	0.0081	35.4522	3.555	3.8707
7	2.3541	0.0898	0.0081	34.6471	3.1711	5.8588

The classification is required since the results from segmentation is inadequate. Nevertheless, we initially gather the feature extraction of the image. The trained data which we have is compared with the actual data. The trained data is matched to the various parameters. On basis of the data acquired from the result the categorization is carried out. The parameters analyse the train data and classify the picture depending on the textive features of the image. It is discovered using the parameters that determines whether the tumor is benign or a malignant.

3.4 Classification

In Classification the analysis of the presence or absence of tumour is implemented. It is presented in form of Confusion matrix (Çinar et al, 2020). It is a popular depiction for evaluating a classification technique's effectiveness. It may also be employed to examine the outcomes of a technique. The four Confusion matrix is presented below.

Table 3. Confusion Matrix for Cuckoo search algorithm using Otsu as an objective function

Total Images - 340 Tumor Images – 220 No Tumor Images - 120		Predicted		
		With Benign Tumor	With Malignant Tumor	NO Tumor
Actual	With Benign Tumor	120	06	04
	With Malignant Tumor	06	80	04
	NO Tumor	08	06	106

Table 4. Confusion Matrix for Cuckoo search algorithm using Kapur entropy as an objective function

Total Images - 340 Tumor Images – 220 No Tumor Images - 120		Predicted		
		With Benign Tumor	With Malignant Tumor	NO Tumor
Actual	With Benign Tumor	124	03	03
	With Malignant Tumor	04	82	04
	NO Tumor	06	04	110

Table 5. Confusion Matrix for Cuckoo search algorithm using Tassllias entropy as an objective function

Total Images - 340 Tumor Images – 220 No Tumor Images - 120		Predicted		
		With Benign Tumor	With Malignant Tumor	NO Tumor
Actual	With Benign Tumor	127	01	02
	With Malignant Tumor	03	85	02
	NO Tumor	05	03	112

Table 6. Confusion Matrix for Proposed method using Cuckoo search algorithm

Total Images - 340 Tumor Images – 220 No Tumor Images - 120		Predicted		
		With Benign Tumor	With Malignant Tumor	NO Tumor
Actual	With Benign Tumor	128	01	01
	With Malignant Tumor	01	88	01
	NO Tumor	04	02	114

In Table 3 is the Confusion Matrix for Cuckoo search algorithm using Otsu as an objective function is implemented. In Table 4 is the Confusion Matrix for Cuckoo search algorithm using Kapur entropy as an objective function is implemented. In Table 5 is the Confusion Matrix for Cuckoo search algorithm using Tasslias as an objective function is implemented. In Table 6 is the Confusion Matrix for proposed method using Cuckoo search algorithm is implemented.

It is seen that totally 340 images are taken into consideration. There are 220 tumor images, in this 130 images are begine type tumor and 90 images are malignant type tumor, and 120 are non-tumor images. From the confusion matrix, True Positive(TP), False Positive(FP), True Negative(TN) and False Negative(FN) for begine tumor, malignant tumor and no tumor is found.

1. TP(Begine) : True Positive (Begine) refers if the input images are considered as a begine tumor then images are classified as a begine tumor.
2. TP(Malignant) : True Positive (Malignant) refers if the input images are considered as a malignant tumor then images are classified as a malignant tumor.
3. TP(No Tumor) : True Positive (No Tumor) refers if the input images are considered as a no tumor then images are classified as a no tumor.

4. FP(Begine) : False Positive(Begine) refers if the input images are considered as a malignant tumor or no tumor then images are classified as a begine tumor.
5. FP(Malignant) : False Positive(Malignat) refers if the input images are considered as a begine tumor or no tumor then images classified as a malignant tumor.
6. FP(No Tumor) : False Positive(No Tumor) refers if the input images are considered as a begine tumor or malignant tumor then images classified as a no tumor.
7. TN(Begine) : True Negative(Begine) refers if the input images are considered as a malignant tumor or no tumor then images classified as a malignant tumor or no tumor but not classified as a begine tumor.
8. TN(Malignant) : True Negative(Malignant) refers if the input images are considered as a begine tumor or no tumor then images classified as a begine tumor or no tumor but not classified as a malignant tumor.
9. TN(No Tumor) : True Negative(No Tumor) refers if the input images are considered as a begine tumor or malignant tumor then images classified as a begine tumor or malignant tumor but not classified as a no tumor.
10. FN(Begine) : False Negative(Begine) refers if the input images are considered as a begine tumor then images classified as a malignant tumor or no tumor.
11. FN(Malignant) : False Negative(Maligant) refers if the input images are considered as a maglinant tumor then images classified as a begine tumor or no tumor.
12. FN(No Tumor) : False Negative(No Tumor) refers if the input images are considered as a no tumor then images classified as a begine tumor or malignant tumor.

Table 7. True Positive(TP), False Positive(FP), True Negative(TN) and False Negative(FN) for begine tumor, malignant tumor and no tumor

	Cuckoo search algorithm using Otsu as an objective function	Cuckoo search algorithm using Kapur entropy as an objective function	Cuckoo search algorithm using Tassllias entropy as an objective function	Proposed method using Cuckoo search algorithm
TP(Begine)	120	124	127	128
TP(Malignant)	80	82	85	88
TP(No Tumor)	106	110	112	114
FP(Begine)	14	10	08	05
FP(Malignant)	12	07	04	03
FP(No Tumor)	08	07	04	02
TN(Begine)	196	200	202	205
TN(Malignant)	238	243	246	247
TN(No Tumor)	212	213	216	218
FN(Begine)	10	06	03	02
FN(Malignant)	10	08	05	02
FN(No Tumor)	14	10	08	06

In Table 7, the value of True Positive(TP), False Positive(FP), True Negative(TN) and False Negative(FN) for begine tumor, malignant tumor and no tumor for cuckoo search algorithm using different objective functions; like; ostu, kapur entropy, tasslias entropy, as well as proposed method using cuckoo search algorithm are described.

The confusion matrix of classification is presented above. There are five performance assessments that are being considered in the article. They are Sensitivity (Se), Specificity (Sp), Positive Predictive Value (PPV), Negative Predictive Value (NPV) & Accuracy (Acc) (Kalpana, R et al, 2020). The performance assessment of proposed system is analysed & their equations are presented below.

$$Sensitivity\ (S_e) = \frac{TP}{TP+FN} \quad (29)$$

$$Specificity\ (S_p) = \frac{TN}{FP+TN} \quad (30)$$

$$Positive\ Predictive\ Value\ (PPV) = \frac{TP}{TP+FP} \quad (31)$$

$$Negative\ Predictive\ Value\ (NPV) = \frac{TN}{TN+FN} \quad (32)$$

$$Accuracy\ (Acc) = \frac{TP+TN}{TP+FN+TN+FP} \quad (33)$$

Table 8. Comparision of different objective function using cuckoo search algorithm in terms of parameters for tumor detection

	Cuckoo search algorithm using Otsu as an objective function	Cuckoo search algorithm using Kapur entropy as an objective function	Cuckoo search algorithm using Tassllias entropy as an objective function	Proposed method using Cuckoo search algorithm
Se(Begine Tumor)	0.92308	0.95385	0.97692	0.98462
Se(Malignant Tumor)	0.88889	0.91111	0.94444	0.97778
Se(No Tumor)	0.88333	0.91667	0.93333	0.95000
Sp(Begine Tumor)	0.93333	0.95238	0.96190	0.97619
Sp(Malignant Tumor)	0.95200	0.97200	0.98400	0.98800
Sp(No Tumor)	0.96363	0.96818	0.98181	0.99090
PPV(Begine Tumor)	0.89552	0.92537	0.94074	0.96241
PPV(Malignant Tumor)	0.86957	0.92135	0.95506	0.96703
PPV(No Tumor)	0.92982	0.94017	0.96552	0.98276
NPV(Begine Tumor)	0.95145	0.97087	0.98536	0.99033
NPV(Malignant Tumor)	0.95967	0.96812	0.98000	0.99196
NPV(No Tumor)	0.93805	0.95515	0.96428	0.97321
ACC(Begine Tumor)	0.92941	0.95294	0.96764	0.97941
ACC(Malignant Tumor)	0.93529	0.95588	0.97352	0.98529
ACC(No Tumor)	0.93529	0.95000	0.96470	0.97647
ACC(all)	0.90000	0.92941	0.95294	0.97059

In Table 8, five different parameters using confusion matrix are found for different methods. In first method, in the segmentation part, multi-thresholding cuckoo algorithm using ostu as an objective function used. In second method, in the segmentation part, multi-thresholding cuckoo algorithm using kapur entropy as an objective function used. In third method, in the segmentation part, multi-thresholding cuckoo algorithm using Tsallis entropy as an objective function used In the proposed multi-thresholding cuckoo algorithm combined ostu and Tsallis entropy used as an objective function that gives best output for all parameters.

4. CONCLUSION

The research activity consists of several stages, including Pre-processing, Segmentation, Feature Extraction and Classification. In Pre-processing process individual and combination of filters like Median filter, Weiner filter, Anisotropic filter, NLM, Weiner and NLM, Weiner and Anisotropic and Weiner and Median has been described. Combination of Weiner and Anisotropic Filter generated optimum result. Various thresholding, entropy, and evolutionary techniques, such as Two-level thresholding, Multilevel thresholding, Otsu's method, Kapur's entropy method, Tsallis entropy method & Cuckoo search (CS) algorithm, Lévy flight modelling are detailed in segmentation. It is observed that the Cuckoo Otsu & Tsallise Threshold combination delivers outstanding outcome in segmentation. In Feature Extraction various approaches like Stationary Wavelet Transform (SWT) and Discrete Wavelet Transform (DWT) are employed. Three fourty images were taken into account for MRI scan and numerous parameters were discussed, in this patient data taken into the DICOM format from the imagine centre are taken from internet. Since Segmentation cannot generate an accurate outcome and hence Feature extraction is utilized. Based on textive feature of an image the parameters are compared to trained data and then its classification is done. Regarding Classification methodology like Support vector machine (SVM), K Nearest Neighbors KNN, Convolutional Neural Network CNN were described. The Confusion matrix and various filter combinations are deployed for detecting tumors. The parameters like Sensitivity, Specificity, Positive Predictive Value (PPV), Negative Predictive Value (NPV) & Accuracy (Acc) of combination of filters are compared with help of True Positive, True Negative, False Positive & False Negative. The combination of (Weiner + Anistropic) + Cuckoo combined {Ostu+ Tsallis } + DWT + SVM delivers excellent result. The proposed methodology reflects the effective way to identify the nature of brain tumors along with adequate MRI scan.

Acknowledgment: We would like to thanks the Sahyog Imaging Centre, SSG Hospital, Baroda Medical College, The Maharaja Sayajirao University of the Baroda, Vadodara, Gujarat, India, for providing patients Brain DICOM Images.

References:

Anoop, V., & Bipin, P. R. (2019). Medical Image Enhancement by a Bilateral Filter Using Optimization Technique. *Journal of Medical Systems, 43*(8). doi: 10.1007/s10916-019-1370-x

Buades, A., Coll, B., & Morel, J. M. (2005). A Review of Image Denoising Algorithms, with a New One. Multiscale Modeling &Amp. *Simulation, 4*(2), 490–530. doi: 10.1137/040616024

Chahal, P. K., Pandey, S., & Goel, S. (2020). A survey on brain tumor detection techniques for MR images. *Multimedia Tools and Applications, 79*(29–30), 21771–21814. doi: 10.1007/s11042-020-08898-3

Çinar, A., & Yildirim, M. (2020). Detection of tumors on brain MRI images using the hybrid convolutional neural network architecture. *Medical Hypotheses, 139*, 109684. doi: 10.1016/j.mehy.2020.109684

Deng, Q., Shi, Z., & Ou, C. (2022). Self-Adaptive Image Thresholding within Nonextensive Entropy and the Variance of the Gray-Level Distribution. *Entropy, 24*(3), 319. doi: 10.3390/e24030319

Gayathri, S., Wise, D. J. W., Janani, V., Eleaswari, M., & Hema, S. (2020). Analyzing, Detecting and Automatic Classification of Different Stages of Brain Tumor Using Region Segmentation and Support Vector Machine. 2020 *International Conference on Electronics and Sustainable Communication Systems (ICESC)*. doi: 10.1109/icesc48915.2020.9156057

Huang, Z., Ou, C., Lin, B., Su, G., & Chen, J. (2013). The available force in long-duration memory complex systems and its statistical physical properties. *EPL (Europhysics Letters), 103*(1), 10011. doi: 10.1209/0295-5075/103/10011

Jia, Z., & Chen, D. (2020). Brain Tumor Identification and Classification of MRI images using deep learning techniques. IEEE Access, 1–1. doi: 10.1109/access.2020.3016319

Jude Hemanth, D., & Anitha, J. (2012). Image Pre-processing and Feature Extraction Techniques for Magnetic Resonance Brain Image Analysis. *Communications in Computer and Information Science*, 349–356. doi: 10.1007/978-3-642-35594-3_47

Kalpana, R., & Chandrasekar, P. (2020). An optimized technique for brain tumor classification and detection with radiation dosage calculation in MR image. *Microprocessors and Microsystems, 72*, 102903. doi: 10.1016/j.micpro.2019.102903

Kapur, J., Sahoo, P., & Wong, A. (1985). A new method for gray-level picture thresholding using the entropy of the histogram. *Computer Vision, Graphics, and Image Processing, 29*(3), 273–285. doi: 10.1016/0734-189x(85)90125-2

Khairuzzaman, A. K. M., & Chaudhury, S. (2019). Masi entropy based multilevel thresholding for image segmentation. *Multimedia Tools and Applications, 78*(23), 33573–33591. doi: 10.1007/s11042-019-08117-8

Maheshan, C. M., & Prasanna Kumar, H. (2019). Performance of image pre-processing filters for noise removal in transformer oil images at different temperatures. *SN Applied Sciences, 2*(1). doi: 10.1007/s42452-019-1800-x

Mahmud Boby, S., & Sharmin, S. (2021). Medical Image Denoising Techniques against Hazardous Noises: An IQA Metrics Based Comparative Analysis. *International Journal of Image, Graphics and Signal Processing, 13*(2), 25–43. doi: 10.5815/ijigsp.2021.02.03

Nagarajan, I., & Lakshmi Priya, G. (2019). Removal of noise in MRI images using a block difference-based filtering approach. *International Journal of Imaging Systems and Technology, 30*(1), 203–215. doi: 10.1002/ima.22361

Otsu, N. (1979). A Threshold Selection Method from Gray-Level Histograms. *IEEE Transactions on Systems, Man, and Cybernetics, 9*(1), 62–66. doi: 10.1109/tsmc.1979.4310076

Ou, C., El Kaabouchi, A., Chen, J., Le Méhauté, A., & Wang, A. Q. (2010). Generalized Measure Of Uncertainty And The Maximizable Entropy. *Modern Physics Letters B, 24*(09), 825–831. doi: 10.1142/s0217984910022883

Perona, P., & Malik, J. (1990). Scale-space and edge detection using anisotropic diffusion. *IEEE Transactions on Pattern Analysis and Machine Intelligence, 12*(7), 629–639. doi: 10.1109/34.56205

Pun, T. (1981). Entropic thresholding, a new approach. *Computer Graphics and Image Processing, 16*(3), 210–239. doi: 10.1016/0146-664x(81)90038-1

Rahaman, J., & Sing, M. (2021). An efficient multilevel thresholding based satellite image segmentation approach using a new adaptive cuckoo search algorithm. *Expert Systems With Applications, 174*, 114633. doi: 10.1016/j.eswa.2021.114633

Ramírez-Reyes, A., Hernández-Montoya, A., Herrera-Corral, G., & Domínguez-Jiménez, I. (2016). *Determining the Entropic Index q of Tsallis Entropy in Images through Redundancy. Entropy, 18*(8), 299. doi: 10.3390/e18080299

Rao, C. S., & Karunakara, K. (2022). Efficient Detection and Classification of Brain Tumor using Kernel based SVM for MRI. Multimedia Tools and Applications, 81(5), 7393–7417. doi: 10.1007/s11042-021-11821-z

Raut, M. A. et al. (2016). Texture Parameters Extraction of Satellite Image. *IJSTE-International Journal of Science Technology & Engineering, 2*(1), 13-18.

Suresh, S., & Lal, S. (2016). An efficient cuckoo search algorithm based multilevel thresholding for segmentation of satellite images using different objective functions. *Expert Systems With Applications*, *58*, 184–209. doi: 10.1016/j.eswa.2016.03.032

Tsallis, C. (1988). Possible generalization of Boltzmann-Gibbs statistics. *Journal of Statistical Physics*, *52*(1–2), 479–487. doi: 10.1007/bf01016429

Tsallis, C., Mendes, R., & Plastino, A. (1998). The role of constraints within generalized nonextensive statistics. *Physica A: Statistical Mechanics and Its Applications*, *261*(3–4), 534–554. doi: 10.1016/s0378-4371(98)00437-3

Vadmal, V., Junno, G., Badve, C., Huang, W., Waite, K. A., & Barnholtz-Sloan, J. S. (2020). MRI image analysis methods and applications: an algorithmic perspective using brain tumors as an exemplar. *Neuro-Oncology Advances*, *2*(1). doi: 10.1093/noajnl/vdaa049

Yang, X. S., & Suash Deb. (2009). Cuckoo Search via Lévy flights. 2009 *World Congress on Nature &Amp; Biologically Inspired Computing (NaBIC)*. doi: 10.1109/nabic.2009.5393690

Bhavna Pancholi
Department of Electrical Engineering,
The Maharaja Sayajirao University of Baroda,
Vadodara, Gujarat,
India
bhavana.p.pancholi-eed@msubaroda.ac.in
ORCID: 0000-0002-8908-0590

Pramod Modi
Department of Electrical Engineering,
The Maharaja Sayajirao University of Baroda,
Vadodara, Gujarat,
India
p.s.modi-eed@msubaroda.ac.in
ORCID: 0000-0002-2651-8743

Nehal Chitaliya
Department of Electrical Engineering,
The Maharaja Sayajirao University of Baroda,
Vadodara, Gujarat,
India
nehal_chitaliya@yahoo.co.in
ORCID: 0000-0003-3699-2542